

See discussions, stats, and author profiles for this publication at: <https://www.researchgate.net/publication/26693623>

# Fundamental Optical Properties of Linear and Cyclic Alkanes: VUV Absorbance and Index of Refraction

ARTICLE *in* THE JOURNAL OF PHYSICAL CHEMISTRY A · AUGUST 2009

Impact Factor: 2.69 · DOI: 10.1021/jp903435c · Source: PubMed

---

CITATIONS

18

---

READS

154

9 AUTHORS, INCLUDING:



Brian K Long

University of Tennessee

22 PUBLICATIONS 347 CITATIONS

SEE PROFILE



Steffen Jockusch

Columbia University

220 PUBLICATIONS 6,209 CITATIONS

SEE PROFILE



Alan Campion

University of Texas at Austin

231 PUBLICATIONS 5,410 CITATIONS

SEE PROFILE

# Fundamental Optical Properties of Linear and Cyclic Alkanes: VUV Absorbance and Index of Refraction

Elizabeth A. Costner,<sup>†</sup> Brian K. Long,<sup>‡</sup> Carlos Navar,<sup>†</sup> Steffen Jockusch,<sup>§</sup> Xuegong Lei,<sup>§</sup> Paul Zimmerman,<sup>⊥</sup> Alan Campion,<sup>‡</sup> Nicholas J. Turro,<sup>§</sup> and C. Grant Willson<sup>\*,†,‡</sup>

Department of Chemical Engineering, The University of Texas at Austin, Austin, Texas,

Department of Chemistry, The University of Texas at Austin, Austin, Texas, Department of Chemistry, Columbia University, New York, New York, and SEMATECH, Austin, Texas

Received: April 14, 2009; Revised Manuscript Received: June 15, 2009

VUV absorbance and index of refraction data for a series of linear and cyclic alkanes have been collected in order to understand the relationship between the electronic excitation wavelength (or absorbance edge), index of refraction, and molecular structure. The absorbance edge and index for a homologous series of both linear and cyclic alkanes increase with increasing carbon number. The optical properties of complex cycloalkanes do not vary predictably with increasing carbon number but instead depend on variations in the hydrocarbon structure in addition to hydrocarbon size. An understanding of the fundamental optical properties of this class of compounds is directly applicable to the identification of a high index and low-absorbance fluid for 193 nm immersion lithography.

## 1. Introduction

Alkanes (saturated hydrocarbons) are composed entirely of sigma ( $\sigma$ ) bonds. Electronic transitions in these structures occur at high energies or wavelengths less than 200 nm.<sup>1</sup> The energy (or wavelength) of the electronic transitions depends on the energy difference, or gap, between the highest occupied molecular orbital (HOMO) and lowest unoccupied molecular orbital (LUMO), known as the HOMO–LUMO gap. To understand the trends in the optical properties, such as the absorbance edge and index of refraction, of the alkanes, the nature of the HOMO and LUMO must be understood.

The measurement and understanding of the optical properties of the liquid alkanes are relevant and specifically important for applications such as immersion lithography, a major process used for integrated circuit (IC) fabrication.<sup>2</sup> Immersion lithography is a variation of photolithography,<sup>3</sup> in which a high-index fluid is required to decrease the feature size that can be printed. The semiconductor industry has continually decreased feature sizes by decreasing the exposure wavelength.<sup>4</sup> As technical challenges limit further decreases in the exposure wavelength below 193 nm, inserting a fluid into the light path enables lens designs that effectively decrease the exposure wavelength ( $\lambda_o$ ) by a factor inversely proportional to the index of refraction of the fluid ( $\lambda_{\text{eff}} = \lambda_o/n_f$ ).<sup>2</sup> Thus, a high index fluid, which is transparent at 193 nm, would result in a substantial increase in resolution. Alkanes are ideal candidates for immersion lithography due to their high index of refraction and low absorbance at 193 nm.<sup>5</sup>

Absorbance measurements at short wavelengths (<200 nm) are extremely sensitive to impurities since many compounds exhibit strong absorbances at these wavelengths. Therefore, to

accurately measure the absorbance of a pure alkane fluid, the fluid must be rigorously purified to constant absorbance.<sup>6,7</sup> Additionally, hydrocarbons form weak van der Waals complexes with oxygen that have strong absorption to charge-transfer states above 200 nm.<sup>8</sup> All alkane fluids must be fully deoxygenated prior to absorbance measurement to prevent errors resulting from absorption due to oxygen.

VUV absorbance spectra for a range of linear and cyclic alkanes have been reported in both the liquid and gas phase.<sup>9–15</sup> Trends in both the ionization potential and absorbance of a homologous series of linear alkanes ( $C_1$ – $C_{10}$ ) have received extensive analysis.<sup>14–22</sup> The excited states of cycloalkanes have also been studied, but with less emphasis on the trends in a homologous series.<sup>11,15,20–28</sup> To understand variations in the optical properties and identify structures which provide a high index and low absorbance at 193 nm for immersion lithography, a comprehensive survey of the variation in the absorbance edge of linear, cyclic, and complex cyclic alkanes, with a systematic range of structural variations, is needed. The index of refraction and absorbance of a series of linear, cyclic, and complex cyclic alkanes was therefore studied. Index of refraction data are typically collected and reported in the literature at 589 nm, and liquid-phase absorbance spectra are typically obtained to 200 nm. Therefore, index data at 193 nm and absorbance spectra below 200 nm, for neat fluids, are needed to study the optical properties of the alkanes.

## 2. Experimental Details

**2.1. Materials.** *n*-Pentane [spectrophotometric grade,  $\geq 99\%$  (Acros Organics)], *n*-hexane [ReagentPlus,  $\geq 99\%$  (Aldrich)], *n*-heptane [HPLC,  $\geq 96\%$  (Fisher Chemical)], *n*-octane [ $\geq 99\%$  (Acros Organics)], *n*-decane [ $\geq 99\%$  (Acros Organics)], cyclopentane [purum,  $\geq 98.5\%$  (GC) (Fluka)], cyclohexane [ $\geq 99\%$  (Acros Organics)], cycloheptane [ $>98\%$  (GC) (TCI America)], cyclooctane [ $\geq 99\%$  (Aldrich)], cyclodecane [96+% (Chem-SampCo, Inc.)], methylcyclohexane [ReagentPlus,  $\geq 99\%$  (Sigma–Aldrich)], ethylcyclohexane [ $\geq 99\%$  (Acros Organics)], propylcyclohexane [ $>98\%$  (GC) (TCI America)], butylcyclo-

\* To whom correspondence should be addressed. E-mail: willson@che.utexas.edu.


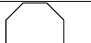
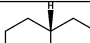
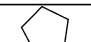
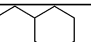
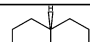
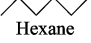
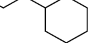
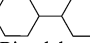
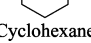
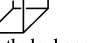

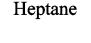
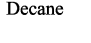
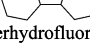
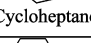
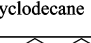
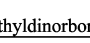
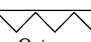
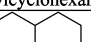


<sup>†</sup> Department of Chemical Engineering, The University of Texas at Austin.

<sup>‡</sup> Department of Chemistry, The University of Texas at Austin.

<sup>§</sup> Columbia University.

<sup>⊥</sup> SEMATECH.

TABLE 1: Structure and Carbon Number of the Alkanes

Structure	Carbon Number	Structure	Carbon Number	Structure	Carbon Number
 Pentane	5	 Cyclooctane	8	 <i>cis</i> -Decalin	10
 Cyclopentane	5	 Ethylcyclohexane	8	 <i>trans</i> -Decalin	10
 Hexane	6	 Propylcyclohexane	9	 Bicyclohexyl	12
 Cyclohexane	6	 Methylcubane	9	 1,3-Dimethyladamantane	12
 Heptane	7	 Decane	10	 Perhydrofluorene	13
 Cycloheptane	7	 Cyclodecane	10	 Methyldinorbornane	13
 Methylcyclohexane	7	 Butylcyclohexane	10		
 Octane	8	 Decalin	10		

hexane [ $\geq 99\%$  (Aldrich)], decalin [*cis* + *trans* mix, anhydrous,  $\geq 99\%$  (Sigma–Aldrich)], *cis*-decalin [ $>98\%$  (GC) (TCI America)], *trans*-decalin [ $>98\%$  (GC) (TCI America)], bicyclohexyl [puriss.,  $\geq 99\%$  (GC) (Fluka)], perhydrofluorene [97% (Aldrich)], 1,3-dimethyladamantane [ $\geq 99\%$  (Acros Organics)], and methylcubane [99% (Boron Molecular)] were purchased at the highest purity available. The structure and carbon number of each of these compounds are given in Table 1. Methyltetraacyclododecane was received from B.F. Goodrich and used without further purification. A palladium on carbon catalyst (10 wt % loading) [Aldrich] was also used.

**2.2. Purification Methods.** Even at the highest-purity, commercially available, alkane fluids exhibit a strong UV absorbance due to impurities. Three purification methods, acid wash,<sup>7</sup> column chromatography,<sup>9</sup> and distillation, were used to decrease the concentration of impurities. Each fluid was purified with at least one of these methods until the absorbance was minimized and constant with respect to further purification. Additionally, alkanes form a weak van der Waals complex with oxygen that is capable of undergoing a charge transfer between the subunits after photon absorption, resulting in a strong absorbance at wavelengths greater than 200 nm.<sup>6–8</sup> Therefore, all of the fluids were deoxygenated by sparging with an inert gas such as N<sub>2</sub> or Ar prior to the measurements. An example of the absorbance of cyclohexane with successive purifications is given in Figure 1. Achieving the ultimate purity level for each hydrocarbon is challenging, despite multiple purification steps. These purification methods are described in more detail in the Supporting Information.

**2.4. VUV Absorbance Measurements.** The absorbance spectra were collected in the liquid phase. Since electronically excited states interact readily with neighboring molecules, fine structure resulting from vibrational and rotational transitions is typically not observed in the condensed phases.<sup>9</sup> However, liquid-phase spectra reveal the absorbance onset and can be used to identify trends based on structure to postulate the nature of the excited state.

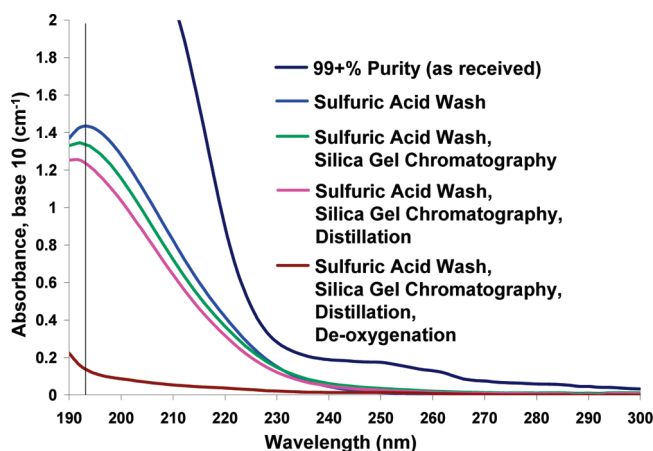


Figure 1. Purification example. Absorbance of spectral-grade cyclohexane (99+% purity) following multiple purification steps

Absorbance spectra were obtained with either an Acton Research Corporation CAMS-507 spectrophotometer from 150 to 250 nm (in a nitrogen-purged environment) or the combination of a modified Varian Cary 400 spectrophotometer from 180 to 200 nm (in a nitrogen-purged environment) and a Shimadzu UV-2401 UV/vis spectrophotometer from 200 to 250 nm. The absorbance edge ( $\lambda_{\text{edge}}$ ) is defined here as the wavelength at which  $A(\text{base } 10) = 2 \text{ cm}^{-1}$ . Decalin (mix, *cis* + *trans*), *cis*-decalin, *trans*-decalin, cyclooctane, cycloheptane, cyclodecane, and methyldinorbornane were measured with the Varian/Shimadzu combination. The remaining fluids were measured with the Acton spectrophotometer. High-purity quartz cells of 1 mm path length from either Hellma–U.S.A. or Starna Cells, Inc. were used for the measurements. Using a 1 mm path length increases the sensitivity of the measurement, so that the absorbance edge can accurately be identified. Methylcubane was measured in a 10 mm path quartz cell from Starna Cells, Inc. from 190 to 250 nm on the Shimadzu spectrophotometer.

To measure the absorbance, a reference spectrum was recorded with no sample cuvette in the light path. The absorbance of a cuvette filled with the sample was then measured. With this method, light lost due to reflections at each of the quartz–air or quartz–fluid interfaces was not accounted for during the experiment. Therefore, the Fresnel equations, which provide a relationship between the transmitted and reflected light at an interface, were combined with Lambert's Law and used to calculate a reflection-corrected absorbance for the sample.

Reflections occur at four interfaces in the light path, the air–quartz interface, the quartz–fluid interface, the fluid–quartz interface, and the quartz–air interface. The transmission of light through each interface is given by the ratio of the intensity of transmitted light ( $I_{ti}$ ) to the intensity of incident light ( $I_{oi}$ ). The Fresnel equations relate transmission and reflection at normal incidence as

$$T_i = 1 - R_i \quad (1)$$

$$T_i = 1 - \left( \frac{n_{ti} - n_{oi}}{n_{ti} + n_{oi}} \right)^2 \quad (2)$$

where  $T_i$  and  $R_i$  are the transmittance and reflectance values at a specific interface ( $i$ ),  $n_{ti}$  is the index of refraction of the material through which the light is transmitted, and  $n_{oi}$  is the index of refraction of the material at which the light is incident. Using the expressions for the transmission of light through each interface and assuming that the quartz is 100% transparent, the value of the transmission of light through the sample can be isolated.

$$\frac{T_{\text{measured}}}{T_1 T_2 T_3 T_4} = T_{\text{sample}} \quad (3)$$

Lambert's Law to calculate the amount of light absorbed by the sample is given by

$$T_{\text{sample}} = 10^{-Az} \quad (4)$$

where  $T_{\text{sample}}$  is the internal transmission, or amount of light transmitted through the sample, corrected for reflection losses,  $A$  is the optical absorbance (base 10) of the sample, and  $z$  is the path length. This equation can be rearranged to solve for the optical absorbance. All optical absorbance values are reported in base 10. Alternatively, a relative transmission method can be used to account for light lost due to reflections by measuring the transmittance of the sample through two different path lengths.<sup>29</sup>

Since the quartz cell is not 100% transparent, a correction for the absorbance of the cell must also be included. To correct for this absorbance, the absorbance spectrum of the empty quartz cell was also measured and corrected for reflections. The reflection-corrected fluid absorbance spectrum was then normalized by the reflection-corrected empty cell absorbance spectrum. Thus, the reflection-corrected empty cell transmission is assumed to be the maximum transmission that can be obtained.

Values of the index of refraction at each interface are needed for this calculation. The index of air is 1 for the entire wavelength range. The index of quartz is well-known with respect to the wavelength and can be obtained from literature

values in the Woollam WVASE32 software. The index of refraction for each of the hydrocarbon samples was measured with the procedure described in section 2.5.

The index of refraction of methylcubane was not collected for the full spectrum and was extrapolated from longer wavelengths. As a result, the absorbance spectrum for this sample is not corrected for reflections. However, since the index values of the quartz cuvette are expected to be similar to those of the fluid, only a small amount of light is lost due to reflections and should result in less than 5% error.

**2.5. Index of Refraction Measurements.** The index of refraction of the fluids was determined from ellipsometric measurements made on a J.A. Woollam M2000 variable angle spectroscopic ellipsometer from 190 to 1000 nm. The ellipsometric parameters  $\Psi$  and  $\Delta$  were fit to a Cauchy dispersion model by the Woollam WVASE32 software. The fluids were measured by filling a 2 in. diameter Fluoroware cup with a curved bottom. Using this method, only reflections from the top surface of the fluid were collected for analysis.<sup>30</sup>

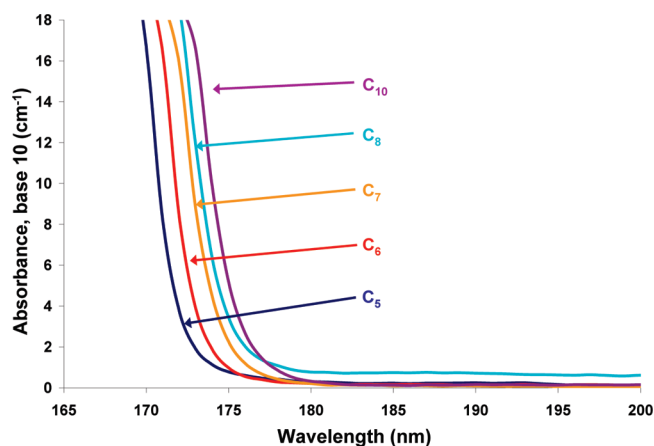
The Cauchy model provides a description of the index of refraction in normal dispersion or wavelengths at which absorption is low. The hydrocarbon fluids were not deoxygenated prior to this index measurement and should have a strong absorption at 193 nm (see Figure 1) such that the Cauchy equation might not accurately model the index. To determine the validity of the Cauchy model, the indexes of deoxygenated and oxygenated samples were compared. Index of refraction values at 193 nm have been reported for deoxygenated decane, cyclohexane, cyclooctane, and decalin (cis + trans, mix), measured using a prism minimum deviation technique, and are 1.549, 1.571, 1.615, and 1.641, respectively.<sup>29,31,32</sup> Without deoxygenation, the index values at 193 nm for decane, cyclohexane, cyclooctane, and decalin (cis + trans, mix) are 1.544, 1.578, 1.611, and 1.654, respectively, according to the Cauchy model fit. Since the index values collected for the deoxygenated and oxygenated fluids are similar, the Cauchy model seems to accurately predict the index, despite the known high absorbance due to dissolved oxygen. When the order of magnitude of the index is much greater than the extinction coefficient (or absorbance), the index dominates the beam reflected from the sample and collected by the detector. Thus, despite the presence of dissolved oxygen, the extinction coefficient must still be much smaller than the index, so that essentially only information about the index is contained in the reflected beam.

### 3. Results and Discussion

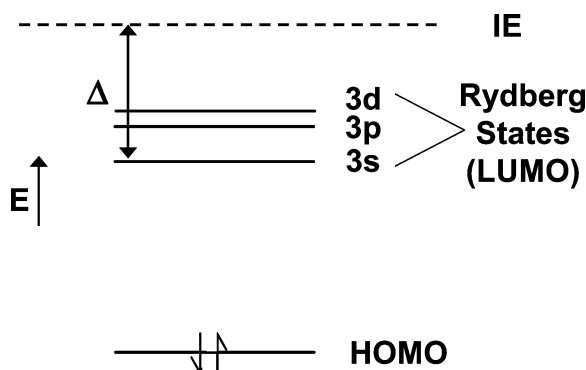
**3.1. Linear Alkane Absorbance Spectra.** The absorbance spectra of the normal alkane series from  $C_5$  to  $C_{10}$  (excluding  $C_9$ ) are given in Figure 2. The absorbance shifts to longer wavelengths (decreases to lower energies) as the number of carbons in the linear chain increases. This absorbance shift suggests that the energy between the HOMO and LUMO (HOMO–LUMO gap) decreases as the number of carbons in the linear chain increases.

To develop a hypothesis for the observed decrease in the HOMO–LUMO gap with the addition of carbon atoms, the change in the energy of the HOMO and LUMO as carbons are added should be evaluated. First, when carbons are added to the linear chain, the added electrons occupy orbitals of increasingly higher energy. With orbitals of higher energies occupied, the energy of the HOMO increases. The increase in the energy of the HOMO with the addition of carbon atoms is known as orbital “destabilization”. With the shift in the HOMO to higher energies, the energy of the LUMO must be either decreased or





**Figure 2.** Absorbance spectra of the linear hydrocarbons,  $C_5$ – $C_{10}$  (excluding  $C_9$ ), where Absorbance ( $\text{cm}^{-1}$ ) =  $-\log_{10}(I/I_0)$ . The baseline observed for  $C_8$  (octane) is likely due to residual impurities.



**Figure 3.** HOMO–LUMO gap in alkanes and Rydberg term value ( $\Delta$ ).

unaffected with increasing carbon number to achieve the observed decrease in the HOMO–LUMO gap.

Robert Mulliken identified that the lowest-energy excited orbitals (LUMO) of these alkane systems are primarily Rydberg in character by studying methane and ethane.<sup>33</sup> A Rydberg orbital is a nonbonding orbital that is not in the valence shell. These orbitals have a much larger radius than that of the core orbitals.<sup>22</sup> Electronic excitations to Rydberg states occur in series and can be identified if their excitation energy (or frequency,  $\omega$ ) fits the Rydberg formula given by

$$\omega = \text{IE} - \frac{R_\infty}{(n - \delta)^2} \quad (5)$$

where IE is the ionization potential toward which the series converges,  $R_\infty$  is the Rydberg constant ( $109737 \text{ cm}^{-1}$ ),  $n$  is the principal quantum number of the Rydberg orbital and can increase to infinity (for alkanes,  $n = 3, 4, 5, \dots$ ), and  $\delta$  is the quantum defect or Rydberg correction.<sup>22</sup> The difference between the ionization potential and Rydberg excitation energy is the term value ( $\Delta$ ) and is illustrated in Figure 3. The first three accessible Rydberg states for the alkanes are 3s, 3p, and 3d; these states are also shown in Figure 3. On the basis of term values calculated from gas-phase spectroscopic data for a range of linear alkanes ( $C_1$ – $C_{10}$ ) and cycloalkanes, including cyclohexane, *trans*-decalin, and adamantane, the term value for each Rydberg state seems to be relatively independent of alkane geometry.<sup>11,17,22,25</sup> For the 3p and 3d Rydberg transition, the term values are approximately 2.2 and 1.6 eV, respectively, regardless

of alkane geometry.<sup>25</sup> The term value for the 3s transition is as large as 3.9 eV for methane but converges to approximately 2.7 eV for the larger alkanes ( $>C_8$ ).<sup>22,25</sup> A mainly constant term value indicates that the position of the LUMO is essentially unaltered by the addition of carbon atoms or other changes in alkane geometry. If the LUMO energy is essentially constant and the HOMO energy is “destabilized” (increased) with the addition of carbon atoms, the HOMO–LUMO gap should decrease as the carbon number is increased.

Assuming the LUMO of the alkanes in this study is a Rydberg state, the energy of the LUMO can be evaluated by comparing the term values of each alkane. The 1 mm path through which the absorbance spectra were measured did not allow measurement of the peak maximum, which would correspond to the lowest-energy Rydberg state and should be the energy used to calculate the term values. Since the energy, or wavelength, of the peak maximum was not detectable through the 1 mm path, the absorbance onset wavelength ( $\lambda_{\text{edge}}$ ), defined as the wavelength at which  $A = 2 \text{ cm}^{-1}$ , was used instead to calculate the term values. For each of these alkanes, the absorbance increases sharply, with only a small variation in wavelength up to  $A \sim 20 \text{ cm}^{-1}$  (maximum  $A$  measured), to form a sharp absorbance edge. Assuming that the absorbance continues to increase sharply up to the peak maximum,  $\lambda_{\text{edge}}$  should be a reasonable approximation for the energy of the peak maximum. If  $\lambda_{\text{edge}}$  reasonably approximates the peak maximum, the selection of  $A = 2 \text{ cm}^{-1}$  to define  $\lambda_{\text{edge}}$  should not significantly alter the calculated term values, and these term values should be consistent with reported term values ( $\sim 3 \text{ eV}$ ).<sup>22,25</sup>

The  $\lambda_{\text{edge}}$ , ionization energies,<sup>34</sup> and term values ( $\Delta$ ) are given in Figure 4 for the linear alkane series. Both the ionization energy and energy of  $\lambda_{\text{edge}}$  decrease with increasing carbon number. From Figure 4, the ionization energy decreases from 10.28 eV (121 nm) for *n*-pentane to 9.65 eV (129 nm) for *n*-decane. The  $\lambda_{\text{edge}}$  energy decreases (or wavelength increases) from 7.2 eV (173 nm) for *n*-pentane to 7 eV (176 nm) for *n*-decane. The term values range from 3.1 eV for *n*-pentane to 2.7 eV *n*-decane. These term values are consistent with the previously reported term values ( $\sim 3 \text{ eV}$ ).<sup>22,25</sup> This consistency suggests that the choice of  $\lambda_{\text{edge}}$  to define the peak maximum is a reasonable approximation.

On the basis of the agreement between the calculated and reported term values, the transitions observed in Figure 2 for the linear alkanes seem to be essentially Rydberg transitions. Due to the similarity in the term values calculated for each alkane in the linear series, the energy of the LUMO seems to be essentially unaltered by the addition of carbon atoms. Rydberg states are large, diffuse orbitals which are not significantly affected by the core electrons. Assuming the LUMO is a Rydberg state, it seems reasonable to postulate that the energy of these diffuse states would not be affected by increasing carbon number. Therefore, the hypothesis that the energy of the LUMO is essentially unaltered while the energy of the HOMO is “destabilized” with the addition of carbon atoms seems to explain the decrease in the HOMO–LUMO gap, or the red shift in the  $\lambda_{\text{edge}}$ , observed with increasing carbon number. Finally, in the condensed phases, Rydberg states are broadened so that the exact nature of the vibronic transitions is not observed. Since the 3s Rydberg state has a much lower oscillator strength than the 3p or 3d states,<sup>17</sup> the observed absorptions are likely some mixture of electronic transitions to the 3s, 3p, and 3d states which are unresolved in the liquid phase. If the absorbance spectra of this linear series were measured through a shorter

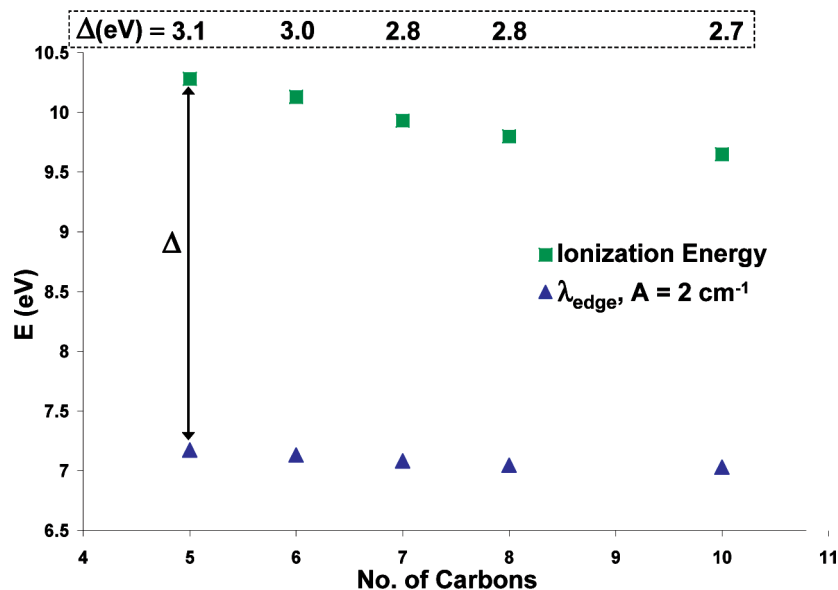


Figure 4. Ionization energies (squares),  $\lambda_{\text{edge}}$  (triangles), and term values ( $\Delta$ ) for the linear alkane series.

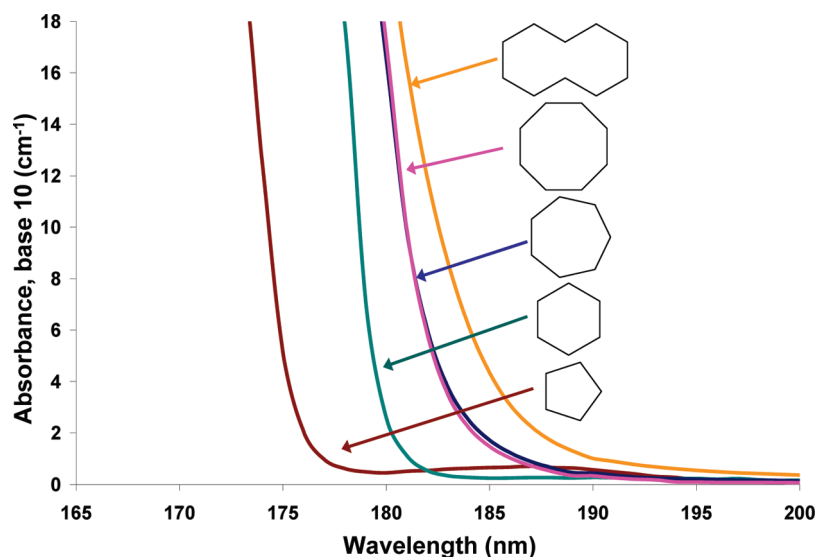


Figure 5. Absorbance spectra for the cycloalkane series  $C_5$ – $C_{10}$  (excluding  $C_9$ ).

path, higher absorption coefficient values could be detected and might further reveal the nature of these Rydberg states.

**3.2. Cycloalkane Absorbance Spectra.** The absorbance spectra of the cycloalkane series ( $C_5$ – $C_{10}$ , excluding  $C_9$ ) are given in Figure 5. As observed for the linear alkanes, the absorbance shifts to longer wavelengths (lower energies) with increasing carbon number, from  $C_5$  to  $C_{10}$ . The term values ( $\Delta$ ) can be calculated for these cyclic structures as in the linear series, using the difference between  $\lambda_{\text{edge}}$  and the ionization energies.<sup>34</sup> The term values, ionization energies, and  $\lambda_{\text{edge}}$  are given in Figure 6.

The ionization energy decreases from 10.33 eV (120 nm) for cyclopentane to 9.6 eV (129 nm) for cyclodecane. The  $\lambda_{\text{edge}}$  energy decreases (or wavelength increases) from 7.1 eV (176 nm) for cyclopentane to 6.6 eV (187 nm) for cyclodecane. The term values for the cycloalkane series range from 3.2 eV for cyclopentane to 3.0 eV for cyclodecane and are consistent with both previously reported term values for the Rydberg state transitions and the term values calculated for the linear series ( $\sim 3$  eV).<sup>22,25</sup> In addition, the term value reported for cyclohexane (3.0 eV) was also calculated in this work.<sup>25</sup> The similarity in

the term values supports the theory that the energy of the LUMO (Rydberg orbital) is essentially unaffected by the geometry of the alkane. If the HOMO is “destabilized” with the addition of carbon atoms, the HOMO–LUMO gap will decrease as the carbon number increases and result in the red shift in the  $\lambda_{\text{edge}}$  with carbon number.

There is a greater shift in  $\lambda_{\text{edge}}$  over the series  $C_5$ – $C_{10}$  for the cycloalkanes than that for the linear alkanes. This shift over a homologous series will be represented by  $\Delta_{\text{shift}}$ ;  $\Delta_{\text{shift}}$  for the cycloalkanes is 11 nm (0.4 eV), while for the linear series,  $\Delta_{\text{shift}}$  is 3 nm (0.1 eV). This difference is illustrated in the plot of  $\lambda_{\text{edge}}$  for both the linear and cyclic alkanes and is given in Figure 7. Additionally, the  $\lambda_{\text{edge}}$  difference between structures of the same carbon number (i.e.,  $n$ -hexane and cyclohexane) also seems to increase as the carbon number increases.

Increasing strain energy shifts the HOMO to higher energies and could explain the difference in  $\Delta_{\text{shift}}$  between the linear and cyclic homologues. However, the strain energies of the cycloalkanes do not increase monotonically with carbon number. Cyclopentane has bond angles of  $108^\circ$ , which differ only slightly from the normal tetrahedral state ( $109.5^\circ$  bond angles) and result

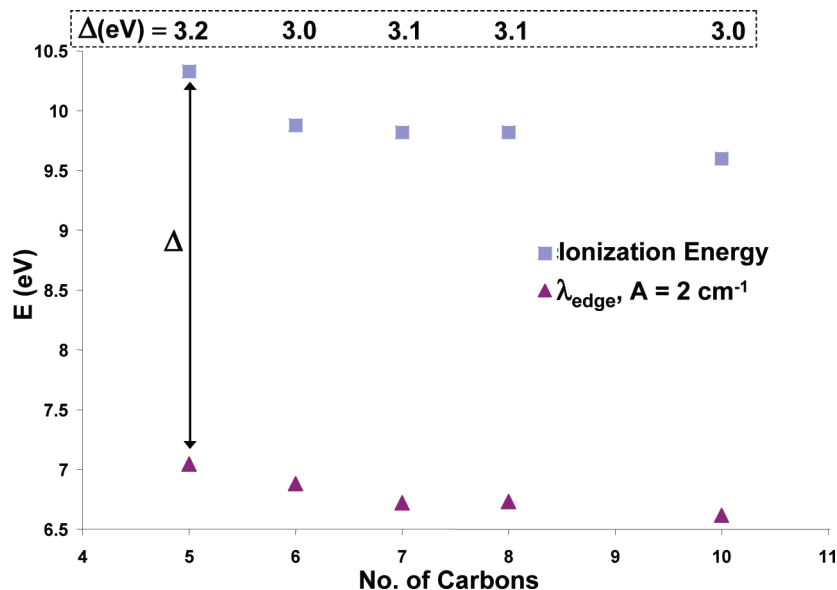


Figure 6. Ionization energies (squares),  $\lambda_{\text{edge}}$  (triangles), and term values ( $\Delta$ ) for the cycloalkanes.

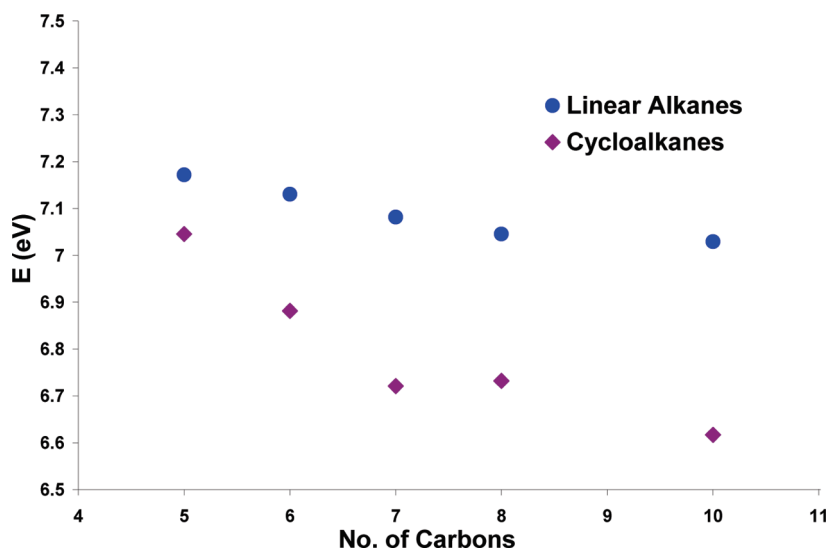


Figure 7. The  $\lambda_{\text{edge}}$  for the linear and cyclic alkanes.

in a small amount of strain energy (27 kJ/mol). Cyclohexane has no ring strain because the “puckering” of the ring allows the achievement of tetrahedral bond angles. Cycloalkanes larger than cyclohexane exhibit a small degree of ring strain, which increases with ring size up to C<sub>9</sub>. The ring strain in cycloheptane is 27 kJ/mol, 42 kJ/mol in cyclooctane, and 50 kJ/mol in cyclodecane.<sup>35</sup> Therefore, an increase in the energy of the HOMO with increased strain energy does not seem to fully explain the difference in  $\Delta_{\text{shift}}$  for the linear and cyclic alkanes, primarily due to the lack of strain in cyclohexane. The difference in  $\lambda_{\text{edge}}$  between linear and cyclic structures with the same carbon number is also not fully explained by strain energy differences since *n*-hexane and cyclohexane would then have the same  $\lambda_{\text{edge}}$  since both structures have no strain energy.

Instead of evaluating strain energies, the difference in ionization energies for the linear and cyclic homologues might provide an explanation for the difference observed in  $\Delta_{\text{shift}}$  and  $\lambda_{\text{edge}}$  for the linear and cyclic structures. However, the large difference in  $\Delta_{\text{shift}}$  and the energies of  $\lambda_{\text{edge}}$  is not observed in the ionization energies. The ionization energies of both the linear and cyclic alkanes are shown in Figure 8. The range in ionization energies is approximately the same for both the linear and cyclic

homologues. While there is some variation in the difference in ionization energy between structures of the same carbon number, this variation does match the trend observed in  $\lambda_{\text{edge}}$ . Therefore, since the ionization energies are not appreciably different for the linear and cyclic structures, the ionization energies do not explain the difference in  $\lambda_{\text{edge}}$ .

The difference in  $\Delta_{\text{shift}}$  and  $\lambda_{\text{edge}}$  observed for the linear and cyclic homologues might be related to differences in dispersion for each of these structures. If the cycloalkanes have a slightly broader absorbance peak than their linear counterparts,  $\lambda_{\text{edge}}$  will red shift slightly. This broadening in the dispersion of the transition for the cyclic structures would explain both the increase in  $\Delta_{\text{shift}}$  and difference in  $\lambda_{\text{edge}}$ . This theory could be evaluated by measuring the absorbance spectra of these homologues in path lengths short enough to reveal the peak maximum.

**3.3. Absorbance Spectra of Alkyl-Substituted Cyclohexanes.** A homologous series of cyclohexane fluids with linear substituents, from methyl to butyl, was also studied. The absorbance spectra for this series are given in Figure 9. The red shift in the absorbance of cyclohexane with the addition of the methyl group is larger than the absorbance shift that occurs with further increases in carbon number (ethyl to butyl).

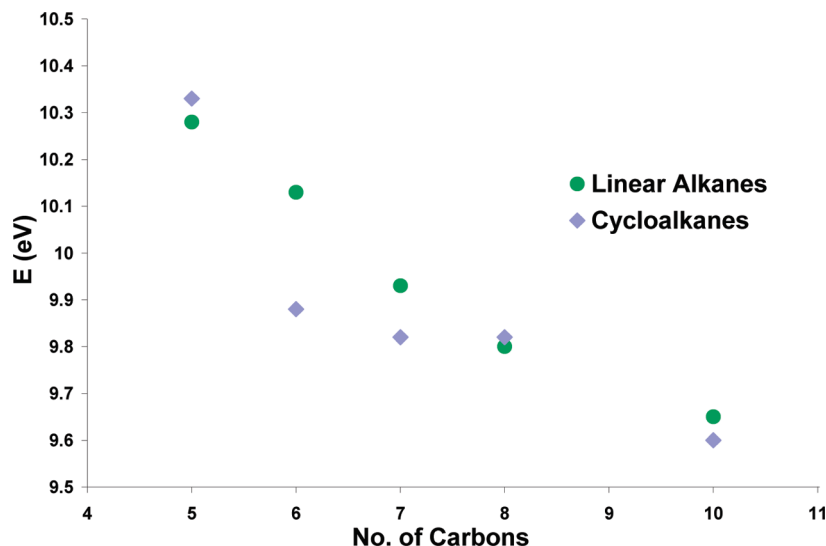


Figure 8. Ionization energies for the linear and cyclic alkanes.

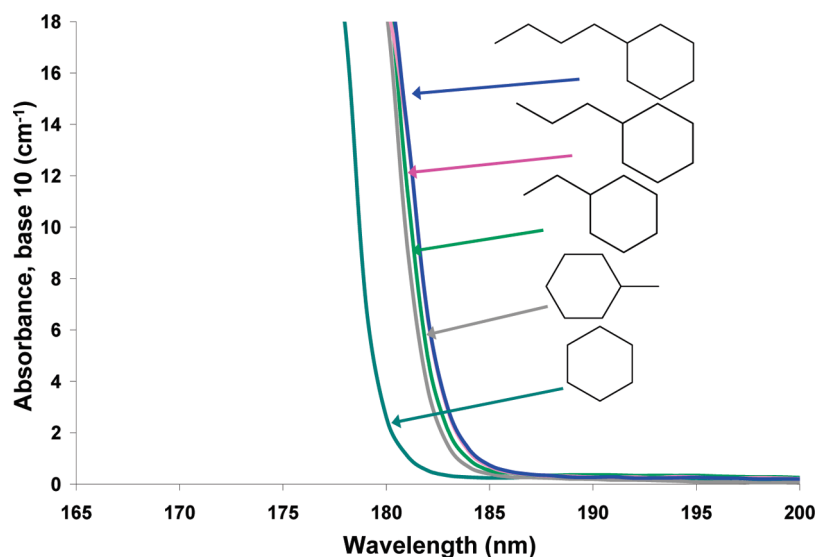


Figure 9. Absorbance spectra for cyclohexane with linear substituents.

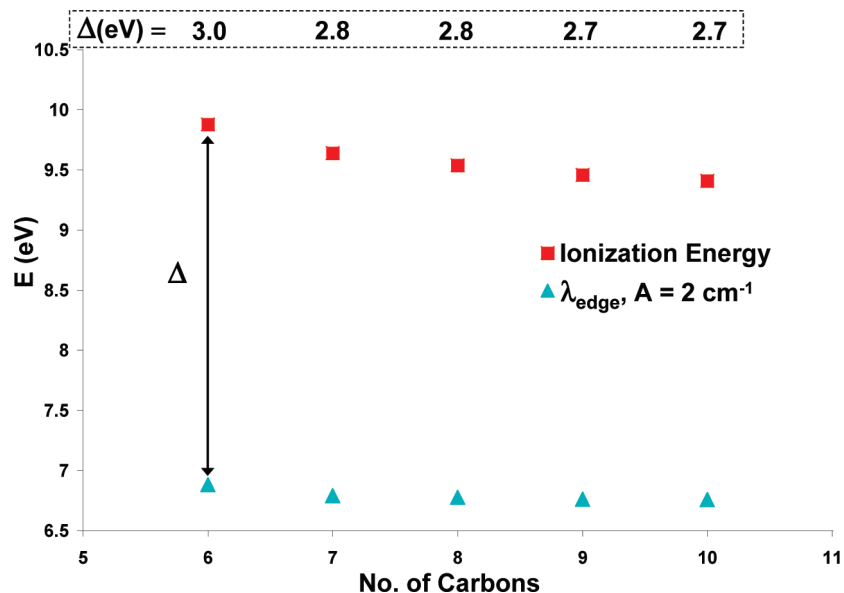
The term values ( $\Delta$ ) can be calculated for these structures as in the linear and cyclic series, using the difference between  $\lambda_{\text{edge}}$  and the ionization energies.<sup>34</sup> The term values,  $\lambda_{\text{edge}}$ , and ionization energies are given in Figure 10. From Figure 10, the ionization energy decreases from 9.88 eV (126 nm) for cyclohexane to 9.64 eV (129 nm) for methylcyclohexane and to 9.41 eV (132 nm) for butylcyclohexane. The  $\lambda_{\text{edge}}$  energy decreases (or wavelength increases) from 6.9 eV (180 nm) for cyclohexane to 6.8 eV (183 nm) for methylcyclohexane. From methylcyclohexane to butylcyclohexane, the  $\lambda_{\text{edge}}$  energy decreases (or wavelength increases) only slightly, from 6.79 (183 nm) to 6.75 eV (184 nm). The term values for this series range from 3.0 eV for cyclohexane to 2.7 eV for butylcyclohexane.

As in the linear and cyclic series, the term values for cyclohexane with linear substituents are consistent with the reported term values for a Rydberg transition.<sup>22,25</sup> The similarity in these term values also supports the theory that the energy of the LUMO (Rydberg orbital) is essentially unaffected by the addition of carbon atoms to the linear chain. With the addition of carbon atoms, the HOMO should be “destabilized” by the increased occupancy of the higher energy orbitals and shift to higher energies, decreasing the HOMO–LUMO gap with increasing carbon number (as in the linear and cyclic series).

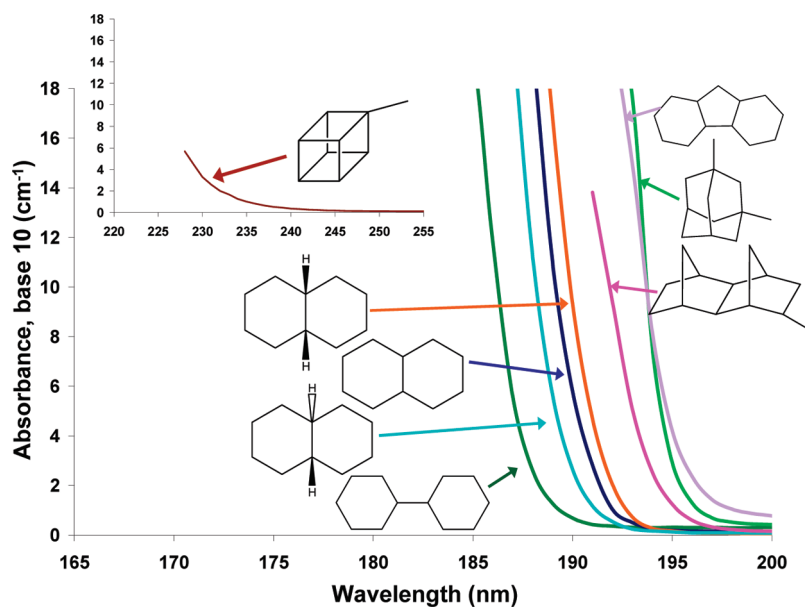
The difference in  $\lambda_{\text{edge}}$  between cyclohexane and methylcyclohexane suggests that addition of the methyl group “destabilizes” the HOMO, as expected based on the increased carbon number. From cyclohexane to methylcyclohexane,  $\Delta_{\text{shift}} = 3$  nm (0.1 eV). From methylcyclohexane to butylcyclohexane, however,  $\Delta_{\text{shift}} = 1$  nm (0.04 eV). Increasing the carbon number of the linear substituent on cyclohexane has essentially no effect on  $\lambda_{\text{edge}}$ , contrary to the trend previously observed for the linear and cyclic series.

Adding a linear substituent to cyclohexane disrupts the symmetry of the six-carbon structure. This change in symmetry might alter which of the Rydberg states (3s, 3p, or 3d) is accessed. If the symmetry disruption is approximately equivalent for each of the structures studied (methyl to butylcyclohexane), then increasing the number of carbons in the *n*-alkane group should not significantly alter  $\lambda_{\text{edge}}$ . If this hypothesis is correct, the dominant factor in the red-shifting  $\lambda_{\text{edge}}$  should be the linear substitution rather than the increase in carbon number with the lengthening of the alkyl chain. To test this hypothesis, the absorbance edge of dimethylcyclohexane could be compared to that of ethylcyclohexane, for example. If the symmetry of cyclohexane is further disrupted,  $\lambda_{\text{edge}}$  for dimethylcyclohexane should be red shifted from ethylcyclohexane.





**Figure 10.** Ionization energies (squares),  $\lambda_{\text{edge}}$  (triangles), and term values ( $\Delta$ ) for cyclohexane ( $\text{C}_6$ ) and methylcyclohexane ( $\text{C}_7$ ) to butylcyclohexane ( $\text{C}_{10}$ ).



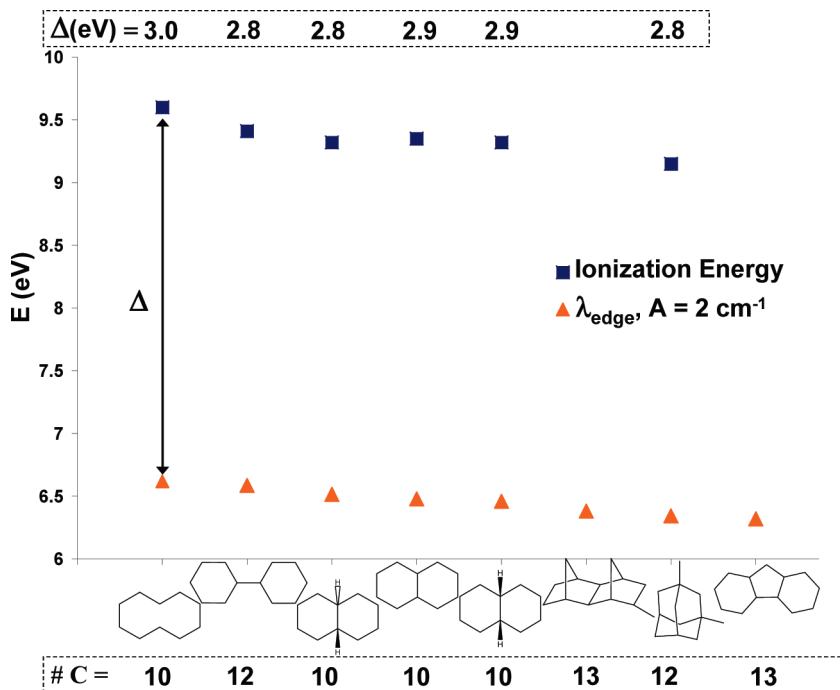
**Figure 11.** Absorbance spectra for the complex cycloalkanes. The spectrum of methylcubane is shown in the inset and was collected through a 10 mm path.

**3.4. Complex Cycloalkane Absorbance Spectra.** The absorbance spectra for some large, complex cycloalkanes are given in Figure 11. For these alkanes, the monotonic red shift in the absorbance with increasing carbon number, as in the linear and cyclic homologues, is not observed. While for these complex cyclic structures a general red shift in the absorbance is observed with increasing carbon number, exceptions to this trend exist. As a result, increasing carbon number does not seem to be the only factor that influences the HOMO–LUMO gap for these cycloalkanes.

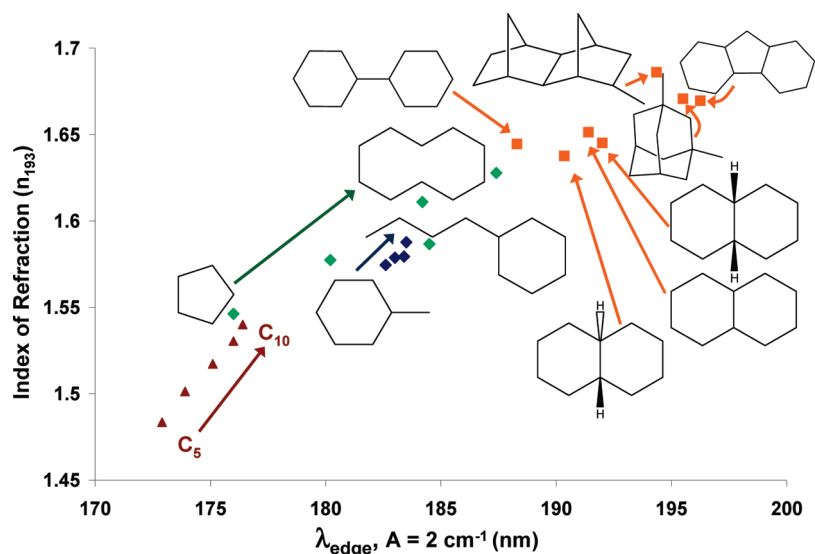
The term values ( $\Delta$ ) can be calculated for these structures using the difference between  $\lambda_{\text{edge}}$  and the ionization energies,<sup>34</sup> as previously discussed. The term values,  $\lambda_{\text{edge}}$ , and ionization energies for the complex cycloalkanes are given in Figure 12. These term values are all approximately 3 eV and are consistent with the reported term values for excitation to Rydberg states.<sup>22,25</sup> Specifically, the reported term value for *trans*-decalin is 2.7 eV<sup>25</sup> and is similar to the term value for *trans*-decalin reported in

this work (2.8 eV). It seems that, as in the alkanes previously discussed, the energy of the LUMO is independent of the structure of the hydrocarbon. The difference in the HOMO–LUMO gap observed for these structures is more likely due to differing amounts of HOMO “destabilization”.

Methylcubane has the lowest-energy  $\lambda_{\text{edge}}$  (longest wavelength) of the fluids studied (5.3 eV, 232 nm), despite consisting of only nine carbons. While the ionization energy of cubane has not been reported, the ionization energy of cubane is 8.6 eV (144 nm).<sup>34</sup> Using the ionization energy of cubane as an approximation for methylcubane, the term value is 3.3 eV and is consistent with the alkane term values ( $\sim 3$  eV) such that the energy of the LUMO is likely approximately equivalent to the LUMO energy of the other alkanes. In methylcubane, six cyclobutane rings are fused into a highly strained cube with internal C–C angles of 90°. Due to the cubic structure, these rings cannot fold to relieve strain; therefore, methylcubane should have significantly higher strain energy than the other



**Figure 12.** Ionization energies (squares),  $\lambda_{\text{edge}}$  (triangles), and term values ( $\Delta$ ) for the complex cycloalkanes; methylcubane,  $\lambda_{\text{edge}} = 5.3$  eV (232 nm).



**Figure 13.** Monotonic relationship between the index at 193 nm and  $\lambda_{\text{edge}}$ .

alkanes. The strain energy of methylcubane is not reported, but the strain energy of cubane is 695 kJ/mol.<sup>36</sup> Increasing strain energies “destabilize” the HOMO, so that the HOMO–LUMO gap of methylcubane should be decreased over unstrained structures, and the absorbance edge should be red shifted.

**3.5. Index of Refraction of Alkanes.** The index of refraction was measured from 190 to 1000 nm. As  $\lambda_{\text{edge}}$  of these alkanes red shifts (with increasing carbon number), the index at 193 nm also increases. Thus, within the linear and cyclic homologous series, a monotonic relationship exists between the optical properties. This relationship is shown in Figure 13 by a plot of the index at 193 nm ( $n_{193}$ ) versus  $\lambda_{\text{edge}}$  (nm). The index and absorbance are linked, and both the index and absorbance increase as the wavelength of incident light approaches an absorption peak.<sup>37</sup> The Cauchy coefficients and index at 193 nm are given in Table 2. The index values at 193 nm for decalin (mix, cis + trans), cis-decalin, and trans-decalin (1.651, 1.645,

and 1.638, respectively) do not seem to follow the simple rule of mixtures. This surprising result likely represents the manifestation of error. The difference in the index of these materials has been previously discussed.<sup>38</sup>

The index of refraction depends on both density and polarizability. One hypothesis for the index dependence on density is related to the “electron density” per unit volume. With greater density and better “packing efficiency” per unit volume, alkanes with higher density will also have higher “electron density”. The interaction of light with an increased number of electrons per unit volume increases the index.<sup>5,39</sup> The polarizability is a measure of the disruption of the charge distribution of a molecule by interaction with an external field. When a nonpolar molecule is subjected to an external electric field, the electrons and nuclei are displaced with respect to each other, creating a dipole moment. The vector sum, or strength, of the dipole moments of all of the molecules in a unit volume is the

TABLE 2: Density, Index of Refraction ( $n_{193}$ ) and Cauchy Coefficients

hydrocarbon	density <sup>a</sup> $\rho$ (g/cm <sup>3</sup> )	index $n_{193}$	Cauchy coefficients <sup>b,c</sup>			mean squared error <sup>d</sup>
			A	B ( $\times 10^3$ )	C ( $\times 10^4$ )	
pentane	0.626	1.484	1.357	0.0022	$9.22 \times 10^{-5}$	2.734
hexane	0.655	1.501	1.363	0.0031	$7.56 \times 10^{-5}$	0.614
heptane	0.684	1.517	1.378	0.0020	$1.18 \times 10^{-4}$	2.785
octane	0.703	1.530	1.388	0.0022	$1.15 \times 10^{-4}$	0.577
decane	0.730	1.544	1.399	0.0024	$1.14 \times 10^{-4}$	1.560
cyclopentane	0.745	1.546	1.400	0.0028	$9.86 \times 10^{-5}$	0.803
cyclohexane	0.779	1.577	1.420	0.0021	$1.40 \times 10^{-4}$	8.683
cycloheptane	0.811	1.587	1.438	0.0026	$1.11 \times 10^{-4}$	2.082
cyclooctane	0.834	1.611	1.443	0.0029	$1.25 \times 10^{-4}$	4.841
cyclodecane	0.854	1.628	1.441	0.0054	$5.82 \times 10^{-5}$	1.910
methylcyclohexane	0.769	1.575	1.416	0.0026	$1.22 \times 10^{-4}$	0.797
ethylcyclohexane	0.788	1.579	1.419	0.0027	$1.22 \times 10^{-4}$	1.354
propylcyclohexane	0.793	1.579	1.423	0.0037	$8.17 \times 10^{-5}$	1.652
butylcyclohexane	0.818	1.588	1.433	0.0025	$1.23 \times 10^{-4}$	1.101
bicyclohexyl	0.864	1.645	1.466	0.0028	$1.45 \times 10^{-4}$	6.503
trans-decalin	0.870	1.638	1.468	0.0021	$1.57 \times 10^{-4}$	3.881
decalin (mix, cis + trans)	0.896	1.651	1.463	0.0015	$2.04 \times 10^{-4}$	5.379
cis-decalin	0.897	1.645	1.466	0.0030	$1.38 \times 10^{-4}$	5.155
perhydrofluorene	0.920	1.670	1.479	0.0043	$1.04 \times 10^{-4}$	0.842
1,3-dimethyladamantane	0.886	1.671	1.465	0.0030	$1.74 \times 10^{-4}$	0.782
methyldinorbornane <sup>e</sup>	0.980	1.687	1.497	0.0036	$1.31 \times 10^{-4}$	1.928
methylcubane <sup>e</sup>	1.1	1.72				

<sup>a</sup> Density obtained from Sigma–Aldrich, unless otherwise noted. <sup>b</sup> Cauchy units are B ( $\mu\text{m}^2$ ) and C ( $\mu\text{m}^4$ ). <sup>c</sup> Cauchy equation is valid to 190 nm. <sup>d</sup> Calculated by the WVASE software to fit the Cauchy parameters. <sup>e</sup> Density evaluated experimentally.

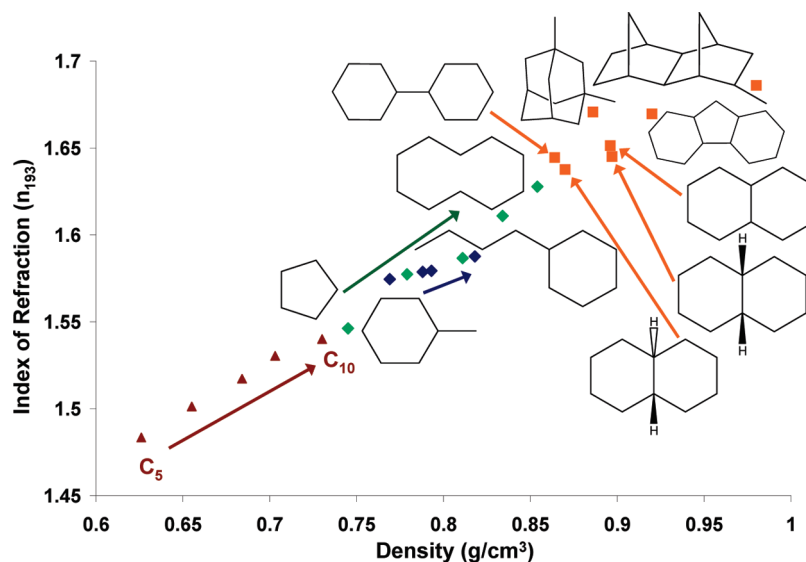


Figure 14. Index of refraction at 193 nm versus density.

polarization. If this external field is light, molecules that are more polarizable will have more ability to decrease the speed of light that passes through the molecule. These more polarizable molecules will have a higher index since the index of refraction describes the change in the speed of light in a medium.<sup>39,40</sup>

The Lorentz–Lorenz formula describes the relationship between the index ( $n$ ), density ( $\rho$ ), and polarizability ( $\alpha$ ) and is given by

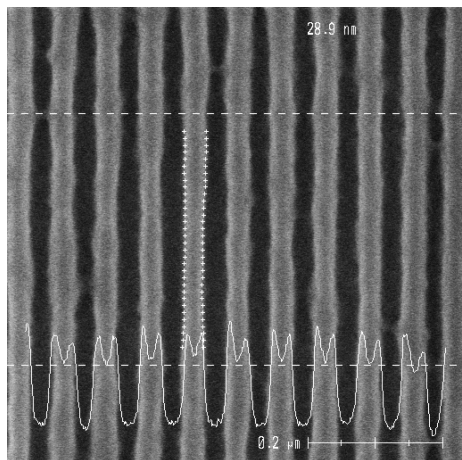
$$\frac{n^2 - 1}{n^2 + 2} = \frac{4\pi N_m \rho \alpha}{3 M_w} \quad (6)$$

where  $N_m$  is Avogadro's number and  $M_w$  is the molecular weight.<sup>39,41</sup> The index at 193 nm increases with increasing density. When the index at 193 nm is plotted against density (shown in Figure 14), an increase in the index with increasing

density is observed, as expected based on eq 6. For the linear alkanes, cycloalkanes, and alkyl-substituted cyclohexanes (methyl to butyl), the index at 193 nm increases monotonically with density. On the basis of eq 6, the polarizability either increases with carbon number or has a negligible effect for these alkanes. For the complex cycloalkanes, the index at 193 nm generally increases with increasing density. Deviations from the trend seem to indicate differences in polarizability for these hydrocarbons.

#### 4. Immersion Lithography

Methyldinorbornane has the highest refractive index of the fluids surveyed ( $n_{193} = 1.687$ ), besides methylcubane. While the transmittance of methyldinorbornane at 193 nm is too low for use in immersion lithography manufacturing, imaging through a thin layer of this fluid is possible with interference immersion lithography<sup>42</sup> and can be used to demonstrate the patterning of 32 nm features with immersion lithography using



**Figure 15.** The 32 nm line and space images printed with methyl dinorbornane as the immersion fluid.

an alkane fluid. The 32 nm line and space images, printed with a numerical aperture of 1.5, are given in Figure 15. These images are of good quality, with few defects and no observable photoresist degradation.

## 5. Conclusions

VUV absorbance spectra of linear and cyclic alkanes reveal that the absorbance edge red shifts with increasing carbon number. This red shift in the absorbance edge suggests that the HOMO–LUMO gap decreases with increasing carbon number. To develop a hypothesis for the appearance of this trend, the nature of the HOMO and LUMO must be established. As electrons are added to orbitals at higher energy states, with increasing carbon number, the energy of the HOMO should increase. On the basis of the agreement between term values reported for alkanes and those calculated in this study (from the difference between the ionization energy<sup>34</sup> and absorbance edge), the excited state (LUMO) for these alkanes seems to be a Rydberg orbital. The term values are essentially constant ( $\sim 3$  eV), despite changes in the alkane geometry, suggesting that the energy of the LUMO is relatively independent of the carbon number. Thus, if the HOMO energy increases with the addition of carbon atoms and the LUMO energy is essentially unaffected, the HOMO–LUMO gap should decrease with increasing carbon number. Exceptions to this trend, observed in the complex cycloalkanes, seem to be primarily due to additional factors which shift the energy of the HOMO, such as an increase in strain energy.

The structural effects required to adjust the optical properties and develop a fluid for next-generation immersion lithography have been characterized. Complex cycloalkanes provide the best option for a high index and low absorbance at 193 nm. Decalin, with an absorbance edge of 191 nm, has the required high index ( $n_{193} = 1.654$ ) and low absorbance needed for a next-generation immersion fluid.

**Acknowledgment.** The authors would like to gratefully acknowledge the Global Research Corporation and Texas Instruments for funding this research. Special thanks to Emil Piscani at SEMATECH for his help with imaging and to Georgia Rich and Alvina Williams at SEMATECH for their assistance with the Acton tool. The authors at Columbia thank the National Science Foundation for its generous support of this research through Grant CHE-07-17518. We also thank the Philanthropic Educational Organization for a scholarship to E.A.C.

**Supporting Information Available:** Additional details about the purification and synthesis of the alkanes tested. This material is available free of charge via the Internet at <http://pubs.acs.org>.

## References and Notes

- (1) Yadav, L. D. S. *Organic Spectroscopy*; Kluwer Academic Publishers: Boston, MA, 2005.
- (2) Lin, B. J. *J. Microlithogr. Microfabr.* **2004**, *3*, 377.
- (3) Thompson, L. F.; Willson, C. G.; Bowden, M. J. *Introduction to Microlithography*, 2nd ed.; American Chemical Society: Washington, DC, 1994.
- (4) Lin, B. J. *Microelectron. Eng.* **2006**, *83*, 604.
- (5) Lopez-Gejo, J.; Kunjappu, J. T.; Zhou, J.; Smith, B. W.; Zimmerman, P.; Conley, W.; Turro, N. J. *Chem. Mater.* **2007**, *19*, 3641.
- (6) Kleven, H. B.; Platt, J. R. *J. Am. Chem. Soc.* **1947**, *69*, 3055.
- (7) Lopez-Gejo, J.; Kunjappu, J. T.; Conley, W.; Zimmerman, P.; Turro, N. J. *J. Micro/Nanolithogr., MEMS, MOEMS* **2007**, *6*, 033003/1.
- (8) Parsons, B. F.; Chandler, D. W. *J. Phys. Chem. A* **2003**, *107*, 10544.
- (9) Kaye, W. I. *Appl. Spectrosc.* **1961**, *15*, 130.
- (10) Pickett, L. W.; Muntz, M.; McPherson, E. M. *J. Am. Chem. Soc.* **1951**, *73*, 4862.
- (11) Raymonda, J. W. *J. Chem. Phys.* **1972**, *56*, 3912.
- (12) Schoen, R. I. *J. Chem. Phys.* **1962**, *37*, 2032.
- (13) Sowers, B. L.; Arakawa, E. T.; Birkhoff, R. D. *J. Chem. Phys.* **1971**, *54*, 2319.
- (14) Lombos, B. A.; Sauvageau, P.; Sandorfy, C. *J. Mol. Spectrosc.* **1967**, *24*, 253.
- (15) Raymonda, J. W.; Simpson, W. T. *J. Chem. Phys.* **1967**, *47*, 430.
- (16) Holmes, J. L.; Lossing, F. P. *Org. Mass Spectrom.* **1991**, *26*, 537.
- (17) Au, J. W.; Cooper, G.; Burton, G. R.; Olney, T. N.; Brion, C. E. *Chem. Phys.* **1993**, *173*, 209.
- (18) Kameta, K.; Kouchi, N.; Ukai, M.; Hatano, Y. *J. Electron Spectrosc.* **2002**, *123*, 225.
- (19) Honig, R. E. *J. Chem. Phys.* **1948**, *16*, 105.
- (20) Potts, A. W.; Streets, D. G. *J. Chem. Soc., Faraday Trans. 2* **1974**, *70*, 875.
- (21) Dewar, M. J. S.; Worley, S. D. *J. Chem. Phys.* **1969**, *50*, 654.
- (22) Robin, M. B. *Higher Excited States of Polyatomic Molecules*; Academic Press: New York, 1974; Vol. 1.
- (23) Bodor, N.; Dewar, M. J. S.; Worley, S. D. *J. Am. Chem. Soc.* **1970**, *92*, 19.
- (24) Heilbronner, E.; Honegger, E.; Zambach, W.; Schmitt, P.; Guenther, H. *Helv. Chim. Acta* **1984**, *67*, 1681.
- (25) Heath, B. A.; Kuebler, N. A.; Robin, M. B. *J. Chem. Phys.* **1979**, *70*, 3362.
- (26) Nesselrodt, D. R.; Potts, A. R.; Baer, T. *Anal. Chem.* **1995**, *67*, 4322.
- (27) Shang, Q. Y.; Bernstein, E. R. *J. Chem. Phys.* **1994**, *100*, 8625.
- (28) Basch, H.; Robin, M. B.; Kuebler, N. A.; Baker, C.; Turner, D. W. *J. Chem. Phys.* **1969**, *51*, 52.
- (29) French, R. H.; Yang, M. K.; Lemon, M. F.; Synowicki, R. A.; Pribil, G. K.; Cooney, G. T.; Herzinger, C. M.; Green, S. E.; Burnett, J. H.; Kaplan, S. G. *Proc. SPIE Int. Soc. Opt. Eng.* **2004**, *5377*, 1689.
- (30) Synowicki, R. A.; Pribil, G. K.; Cooney, G.; Herzinger, C. M.; Green, S. E.; French, R. H.; Yang, M. K.; Burnett, J. H.; Kaplan, S. J. *Vac. Sci. Technol.* **2004**, *22*, 3450.
- (31) French, R. H.; Peng, S.; Wheland, R. C. *Ultraviolet-transparent alkanes and processes using same in vacuum and deep ultraviolet applications*; Co, E. I. D. d. N. a., Ed.; 2005; Patent Version Number: WO/2005/119371.
- (32) French, R. H.; Sewell, H.; Yang, M. K.; Peng, S. P.; McCafferty, D.; Qiu, W.; Wheland, R. C.; Lemon, M. F.; Markoya, L.; Crawford, M. K. *J. Microlithogr. Microfabr. Microsyst.* **2005**, *4*, 031103.
- (33) Mulliken, R. S. *J. Chem. Phys.* **1935**, *3*, 517.
- (34) <http://webbook.nist.gov/>(2009).
- (35) Solomons, T. W. G.; Fryhle, C. B. *Organic Chemistry*, 7th ed.; John Wiley and Sons, Inc: New York, 2000.
- (36) Schleyer, P. v. R.; Williams, J. E., Jr.; Blanchard, K. R. *J. Am. Chem. Soc.* **1970**, *92*, 2377.
- (37) Wooten, F. *Optical Properties of Solids*; Academic Press: New York, 1972.
- (38) Yang, M. K.; Kaplan, S. G.; French, R. H.; Burnett, J. H. *J. Micro/Nanolithogr., MEMS, MOEMS* **2009**, *8*, 023005.
- (39) Born, M.; Wolf, E. *Principles of Optics*, 2nd ed.; Pergamon Press: New York, 1964.
- (40) Korff, S. A.; Breit, G. *Rev. Mod. Phys.* **1932**, *4*, 471.
- (41) Bottcher, C. J. F. *Theory of Electric Polarisation*; Elsevier Publishing Company: London, 1952.
- (42) Smith, B. W.; Bourov, A.; Fan, Y.; Cropanese, F.; Hammond, P. *Proc. SPIE Int. Soc. Opt. Eng.* **2005**, *5754*, 751.